Barrachina Celda, TM.; Garcia-Fenoll, M.; Ánchel Añó, FC.; Miró Herrero, R.; Verdú Martín, GJ.; Pereira ., C.; Da Silva, C.... (2011). REA 3D-dynamic analysis in Almaraz NPP with RELAP5/PARCS v2.7 and SIMTAB cross-sections tables. Progress in Nuclear Energy. 53(8):1167-1180. doi:10.1016/j.bbr.2011.03.031.

REA 3D-DYNAMIC ANALYSIS IN ALMARAZ NPP WITH RELAP5/PARCS v2.7 AND SIMTAB CROSS-SECTIONS TABLES

T. Barrachina[1], M. Garcia-Fenoll[1], F. Anchel[1], R. Miró[1], G. Verdú[1], C. Pereira[2], C. da Silva[2], A. Ortego[3], J. C. Martínez-Murillo[4]

[1]Institute for Industrial, Radiophysical and Environmental Safety (ISIRYM)

Universitat Politècnica de València (UPV)

Camí de Vera s/n, 46021 València, Spain

tebarcel@upvnet.upv.es mfenoll@iqn.upv.es rmiro@iqn.upv.es gverdu@iqn.upv.es

[2]Departamento de Engenharia Nuclear

Universidade Federal de Minas Gerais

Av. Antonio Carlos 6627, 31270-901 Belo Horizonte, Brazil

claubia@nuclear.ufmg.br clarysson_silva@yahoo.com.br

[3]IBERINCO. Avenida de Burgos, Madrid. Spain.

aoi@iberdrola.es

[4]CNAT, Av. Manoteras, Madrid. Spain.

JCMM@cnat.es

ABSTRACT

The Rod Ejection Accident (REA) belongs to the Reactivity- Initiated Accidents (RIA) category of accidents and it is part of the licensing basis accident analyses required for pressurized water reactors (PWR). The REA at hot zero power (HZP) is characterized by a single rod ejection from a core position with a very low power level. The evolution consists basically of a continuous reactivity insertion. The main feature limiting the consequences of the accident in a PWR is the Doppler Effect. To check the performance of the coupled code RELAP5/PARCS v2.7 a REA in Almaraz NPP is simulated. These analyses will allow knowing more accurately the PWR real plant phenomenology in the RIA most limiting conditions.

Keywords: ***RIA analysis, Coupled codes, RELAP5, PARCSv2.7, Fuel enthalpy***

I. INTRODUCTION

The Rod Ejection Accident (REA) belongs to the Reactivity- Initiated Accidents (RIA) category of accidents, and it is part of the licensing basis accident analyses required for pressurized water reactors (PWR). The REA consist of a rod ejection due to the failure of its driving mechanism. The evolution is driven by a continuous reactivity insertion.

We have analyzed the behavior of the Almaraz NPP core in a REA with the coupled neutronic-thermal-hydraulic code RELAP5/PARCSv2.7 [1] [2] using the cross-section set and other kinetic parameters obtained with the application of the SIMTAB methodology [3], developed at UPV. We have studied this transient in different operating conditions and at the beginning and at the end of cycle.

The present work consists of the study of the influence of different definitions of the thermal-hydraulic model in a REA analysis at Almaraz NPP. In previous papers, the authors have studied this transient using a simplified configuration [4] [5]. A series of calculations with different number of thermal-hydraulic channels to represent the core has been made ending in a configuration one to one (one thermalhydraulic channel connected to one radial neutronic node). These channels have been coupled to the neutronic model, developed in a one-to-one basis, that is, each fuel assembly is represented by a radial node in PARCSv2.7 code. The mapping between the thermal-hydraulic and the neutronic model has been performed in different ways to study its influence in the 3D results.

II. DESCRIPTION OF THE MODEL

We have studied the results of the REA analysis at Almaraz NPP operating at Hot Zero Power conditions at the beginning of the cycle and with two different configurations of the control rod positions, rod insertion limit (RIL) and all rods inserted (ARI), using different thermal-hydraulic models.

The reactor core studied contains 157 fuel elements. Each fuel element has 264 fuel rods, 24 guide tubes and 1 tube for the instrumentation. The neutronic nodal discretization consists of 157 x 24 active nodes, considering 13 different types of fuel elements (including one to represent the reflector) with 291 neutronic compositions. The cross-sections tables are generated with the SIMTAB methodology from CASMO4-SIMULATE3 code. A sensitivity analysis, using more compositions and comparing the results with CASMO4-SIMULATE3 code, demonstrates that the considered number of neutronic compositions is adequate.

The neutronic model uses two prompt neutron groups and six delayed neutron groups, while the boundary condition for the neutron diffusion equation is zero-flux at the outer reflector surface.

Radially, the core is divided in 21.504 cm x 21.504 cm cells, each corresponding to one fuel assembly, plus a radial reflector. There are 157 fuel assemblies and 64 reflector assemblies.

Axially, the core is divided into 26 layers (24 fuel layers plus top and bottom reflector) with 15.24 cm height each one, with a total active core height of 365.76 cm.

Using SIMULATE3, the control rod with the maximum worth, for each case, was determined. The results are presented in the Table I.

TABLE I

Control rods are grouped in 6 banks. In the ARI case, initially all the banks are inserted (zero notches of withdrawn), while in the RIL case initially bank 3 is withdrawn at the position 103, bank 4 is totally inserted and the other ones are out of the core (225 notches of withdrawn). One notch is equal to 1.5905 cm. Fig. 1 shows the control rod banks and the ejected rod for each case (highlighted in red for ARI case and highlighted in green for RIL case).

FIGURE 1

Initially, the reactor core has been modeled with 10 thermalhydraulic channels connected with branches (BRANCH) and the by-pass has been modeled as an independent channel (see Fig. 2 and Fig. 3). The thermalhydraulic channels surrounding the ejected control rod have been modeled as independent channels, while the others have been grouped in a unique channel). A time dependent volume (TMDPVOL) and a

time dependent junction (TMDPJUN) simulate the boundary conditions at the entrance and exit of the reactor core as is shown in Fig. 4. Each thermalhydraulic channel representing the core is connected to a heat structure.

FIGURE 2

FIGURE 3

FIGURE 4

Apart from this model, we have analyzed different thermal-hydraulic models in the both cases. In this paper, we present the results from 5 different thermal-hydraulic models for the ARI case. These thermal-hydraulic models have been obtained using the initial model as a reference, increasing the number of the channels surrounding the ejected rod. The total number of thermal-hydraulic channels of each of these models is 26, 12, 13, 14 and 158 respectively. The five models studied are shown in Figs. 5 to 9.

FIGURE 5

FIGURE 6

FIGURE 7

FIGURE 8

FIGURE 9

In the RIL case, we present the results from the initial model besides the model number 6 (Fig. 9). In the RIL case, we have studied only these two models because, as it will be seen in the following sections in the ARI analysis, the maximum and the minimum power during the transient are reached with the initial model and with the 5 different models respectively.

The inlet mass flow through the core is 13301kg/s and it is distributed uniformly among the channels.

The initial steady state is at hot zero power where the moderator density is 742 kg/cm3 and the fuel temperature is 565.583 K. The transient is started by the ejection of the maximum worth rod that is completely extracted in 0.1s.

III. STEADY STATE RESULTS

III.A. Steady State Results with all the Control Rods Inserted

Initial steady state has been simulated with the RELAP5/PARCSv2.7 coupled code. As we have explained before, the parameters used to compare the results with the ones from SIMULATE3 are k_{eff} and axial power profile.

In order to perform the simulation of the model number 6 (with 158 thermal-hydraulic channels) the RELAP5 source code has had to be modified for accepting such a high number of thermal-hydraulic channels.

Figs. 10 to 15 show the power axial profile for the six cases analyzed in the ARI case: initial model and model number 6, the power radial profiles and the radial profile error.

In order to compare the accuracy of the results from RELAP5/PARCSv2.7 with SIMULATE3 between all the cases, we also compare the *Root mean square* (*RMS*) of the power axial profile absolute errors. The comparison of the k_{eff} and *RMS* in the ARI case are summarized in Table II.

TABLE II

FIGURE 10

FIGURE 11

FIGURE 12

FIGURE 13

FIGURE 14

FIGURE 15

Comparing the results, we can observe that the best results in the ARI case are achieved using the model number 6.

III.B. Steady State Results with Control Rods at RIL

The comparison of the k_{eff} and *RMS* in the RIL case is summarized in Table III.

TABLE III

Figs. 16 to 18 show the power axial profile, radial profile and radial profile errors for the initial model analyzed in the RIL case.

FIGURE 16

FIGURE 17

FIGURE 18

IV. TRANSIENT RESULTS

In both cases, ARI and RIL, zero-power state was considered as initial state. The control rod with the maximum worth is ejected in 0.1s. The evolution consists of a continuous reactivity insertion. The Doppler Effect caused by the increase of fuel temperature finishes the transient, but this occurs before it reaches the fuel temperature setpoint that can be dangerous for the nuclear power plant safety, as it expected.

The Doppler temperature (T_f) calculated by PARCSv2.7 code is found from the fuel temperature at the fuel rod center T_{fc} and at the fuel rod surface T_{fs} by the relation:

$$T_f = (1-\alpha)\,T_{fc} + \alpha\,T_{fs} \tag{1}$$

where α is taken equal to 0.7.

IV.A. Transient Results with all the Control Rods Inserted

In the six cases, the initial conditions are at hot zero power. The maximum worth control rod is ejected at 0.1s. The evolution consists of a continuous reactivity insertion. The Doppler Effect caused by the increase of fuel temperature finishes the transient.

Fig. 19 shows the power evolution during the first seconds of the transient in all thecases studied.

FIGURE 19

It can be seen that in all cases a first power peak occurs, followed by a power decrease, until it reaches a plateau value around 750 and 1000 MW. The main difference is the value reached in the power peak. The maximum power peak corresponds to the initial model, while the minimum power peak occurs using the model number 6. To study if the differences in the results could be due to cross flows between channels, we have modified model 2 and model 4 for ARI and RIL, including the cross flow among channels at all axial nodes. Similar results are obtained as for models without the cross flows, concluding that the different results for power and enthalpy evolution is only due to the mapping between the thermalhydraulic and neutronic channels.

Fig. 20 and Fig. 21 show the relative radial power profile at the maximum power for the initial model and the complete model 6. We can see a big difference in the relative radial powers between the channels around the ejected rod and the periphery. Also if we see the

Fig. 14 and Fig. 20 we note that the relative radial powers decrease outside of the hot region and increase in the hot region (channels around the ejected rod). This power deformation is slightly higher for the model 6. These changes in the heat transfer among the channels involve an increase in the moderator temperatures and a decrease in the moderator densities in the channels near the hot one, while the opposite effect occurs in the peripheral channels. Clearly, this decreases the power and maximum enthalpy during the transient. This phenomenon is the cause of the different maximum powers obtained in the simplified and complete models. If we model more accurately the channels outside of the hot region, the negative Doppler reactivity is higher, limiting in this way the power peak.

FIGURE 20

FIGURE 21

Fig. 22 shows the comparison of the enthalpy during the transient in the six cases studied. The maximum enthalpy is reached with the initial model while the minimum is reached with model 6. This phenomenology is normal; if we use a real representation of the thermal-hydraulic of the fuel assemblies, the channels far from the rod ejection channel do not see the reactivity increase, so the power peak and the enthalpy of these channels is quite constant, then the global behavior of the maximum power peak and enthalpy is slower than the initial case. Only one remark, the difference between the maximum power peak and enthalpy for the initial case and the model 6 is very large. This manifest that is very important to simulate all the channels very accurately.

FIGURE 22

The power peak and the maximum enthalpy reached in each case appear in Table IV.

TABLE IV

Table V shows the computational time required in the steady-state and the transient simulations in the ARI cases analyzed. In the coupled steady-state the simulation stops when the steady-state has been reached. The simulation time in the transient is 500s.

TABLE V

IV.B. Transient Results with the Control Rods at RIL

Fig. 23 shows the power evolution during the transient in the models studied.

FIGURE 23

It can be seen that in RIL cases the power increase until it reaches a plateau value. As in the ARI case, the maximum power reached with the model 6 is lower than the obtained with the initial model.

Fig. 24 and Fig. 25 show the relative radial power profile at the maximum power for the initial model and the complete model 6. We can see that the power deformation is higher in the part of the reactor close to the ejected rod. If we compare the Fig. 24 and Fig. 25 we note that the simplified model provides more asymmetric relative radial powers than the complete model 6. Also if we see the Fig. 17 and Fig. 24 we note that the relative radial powers decrease outside of the hot region and increase in the hot region (channels around the ejected rod), but lower than in ARI cases.

FIGURE 24

FIGURE 25

Fig. 26 shows the comparison of the enthalpy during the transient in the two models studied.

FIGURE 26

The power peak and the maximum enthalpy reached in each case appear in Table VI.

TABLE VI

Table VII shows the computational time required in the steady-state and the transient simulations in the RIL cases analyzed:

TABLE VII

V. CONCLUSIONS

In this paper, we have reported the REA 3D dynamic analysis in Almaraz NPP with RELAP5/PARCS v2.7 using the SIMTAB Cross-Sections tables. For that analysis, two different operating conditions at HZP have been studied: first with all control rods inserted and second with control rods at the insertion limit.

The initial steady state is a HZP where the moderator density is 742 kg/cm3 and the fuel temperature is 565.6 K. The transient is started by the ejection of the maximum worth rod that is completely extracted in 0.1 s. The control rod with the maximum worth is different in each of the cases studied.

The evolution of the transient consists of a continuous reactivity insertion. The Doppler Effect caused by the increase of fuel temperature finishes the transient, but this occurs before it reaches the fuel temperature setpoint that can be dangerous for the nuclear power plant safety, as it expected.

The influence of the thermalhydraulic to neutronic mapping in a REA analysis has been studied. The steady state results show a very high accuracy compared with SIMULATE3 in all the studied mappings.

According to the results of the transient simulations, for these cases we can conclude that increasing the number of the thermalhydraulic channels surrounding the control rod that will be ejected, a lower power peak is reached during the transient. The enthalpy evolution during the transient also depends strongly on the number of the thermalhydraulic channels.

The main conclusion of this work is that in order to perform a real analysis of a REA transient in Almaraz NPP under HZP conditions the thermalhydraulic model has to have as many thermalhydraulic channels as the code permits.

ACKNOWLEDGMENTS

This work has been partially supported by the Spanish Ministerio de Educación y Ciencia under project PHB2007-0067-PC and by the Brazilian Coordenação de Aperfeiçoamento de Pessoal de Nível Superior (CAPES) under project CAPES/DGU 159/08.

This work has also been partially supported by the Spanish Ministerio de Educación y Ciencia under project ENE2008-02669, the Generalitat Valenciana under project ACOMP/2009/058, and the Universitat Politècnica de València under project PAID-05-09-4285.

The authors wish to acknowledge the technical and financial support of the Almaraz-Trillo AIE for this work.

REFERENCES

O. Roselló O (2004), *Desarrollo de una metodología de generación de secciones eficaces para la simplificación del núcleo de reactores de agua ligera y aplicación en códigos acoplados neutrónicos termohidráulicos*. PhD Thesis, Universidad Politécnica de Valencia.

CRISSUE-S Partners, (2004), *CRISSUE-S WP1-Report, Neutronics/Thermalhydraulics Coupling in LWR Technology: Data Requirements and Databases Needed for Transient Simulations and Qualification*.

Knott D., Forssén B. H. and Edenius M. (1995), *CASMO-4. A fuel assembly burn-up program*, Studsvik/SOA-95/2.

Cronin J. T., Smith K. S. and Ver Planck D. M. (1995), *SIMULATE-3. Advanced three-dimensional two-group reactor analysis code*, Studsvik/SOA-95/18.

Downar T., Lee D., Xu Y., Kozlowski T. and Staundenmier J. (2004), *PARCSV2.6 US NRC Core Neutronics Simulator*.

Cronin J. T., Smith K. S. and Ver Planck D. M. (1995), *SIMULATE-3. Advanced three-dimensional two-group reactor analysis code*, Studsvik/SOA-95/18.

Fraikin R. and Finnemann H. (1993), *PWR Core Transient Benchmark uncontrolled withdrawal of control rods at zero power*, NEA/NSC/DOC(93)9.

Fraikin R. (1997), *PWR benchmark on uncontrolled rods withdrawal at zero power*, NEA/NSC/DOC(96)20.

Miró R., Maggini F., Barrachina T., Verdú G. (2006), "Analysis of a rod withdrawal in a PWR core with the neutronic-thermalhydraulic coupled code RELAP/PARCS and RELAP/VALKIN", *PHYSOR-2006*, p.9. Vancouver, Canada, 10-14 September.

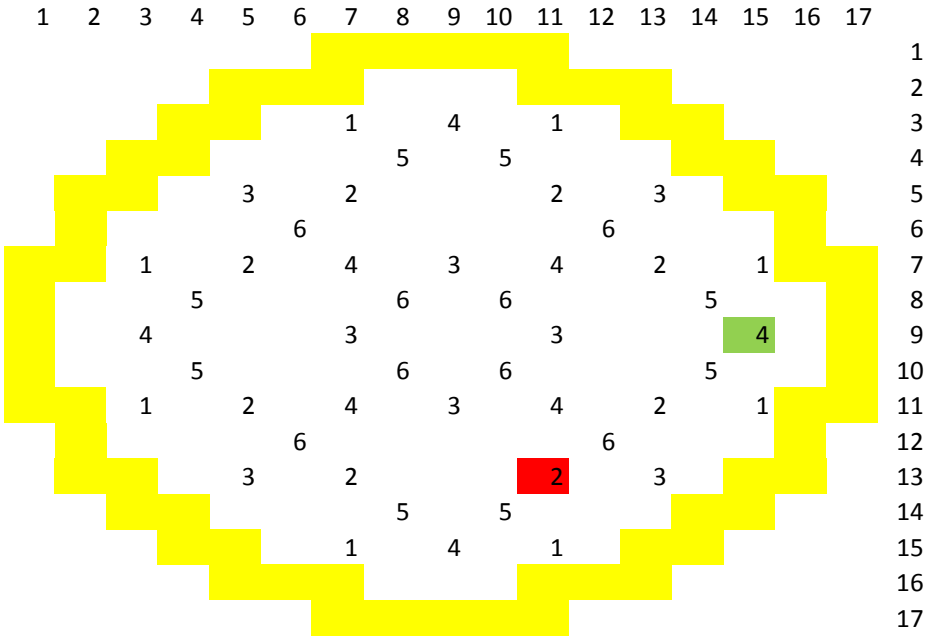

Fig. 1. Control rod banks.

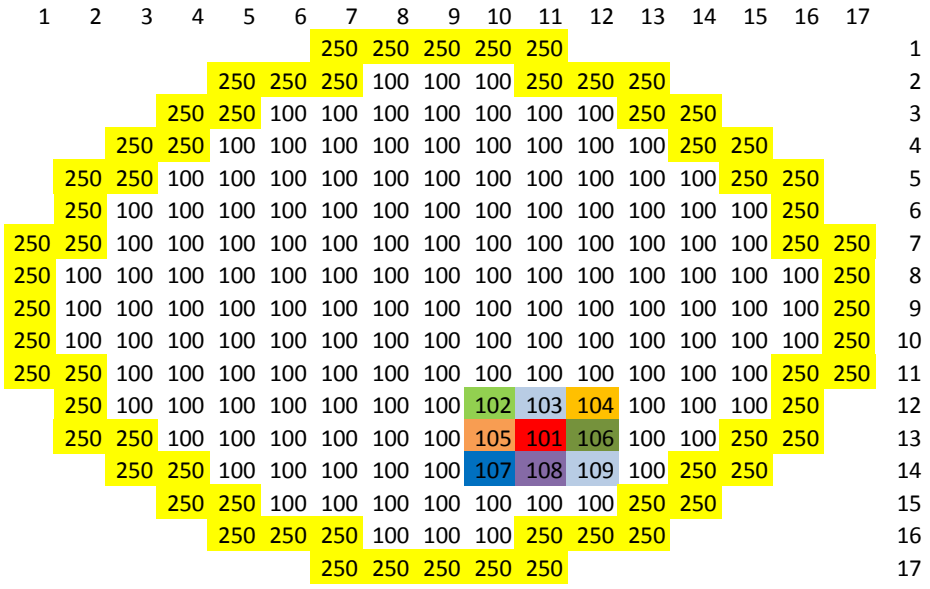

Fig. 2. Thermal-hydraulic channels in the initial model in ARI case.

1	2	3	4	5	6	7	8	9	10	11	12	13	14	15	16	17	
						250	250	250	250	250							1
				250	250	250	100	100	100	250	250	250					2
			250	250	100	100	100	100	100	100	100	250	250				3
		250	250	100	100	100	100	100	100	100	100	100	250	250			4
	250	250	100	100	100	100	100	100	100	100	100	100	100	250	250		5
	250	100	100	100	100	100	100	100	100	100	100	100	100	100	250		6
250	250	100	100	100	100	100	100	100	100	100	100	100	100	100	250	250	7
250	100	100	100	100	100	100	100	100	100	100	100	100	102	103	104	250	8
250	100	100	100	100	100	100	100	100	100	100	100	100	105	101	106	250	9
250	100	100	100	100	100	100	100	100	100	100	100	100	107	108	109	250	10
250	250	100	100	100	100	100	100	100	100	100	100	100	100	100	250	250	11
	250	100	100	100	100	100	100	100	100	100	100	100	100	100	250		12
	250	250	100	100	100	100	100	100	100	100	100	100	100	250	250		13
		250	250	100	100	100	100	100	100	100	100	100	250	250			14
			250	250	100	100	100	100	100	100	100	250	250				15
				250	250	250	100	100	100	250	250	250					16
						250	250	250	250	250							17

Fig. 3. Thermal-hydraulic channels in the initial model in RIL case.

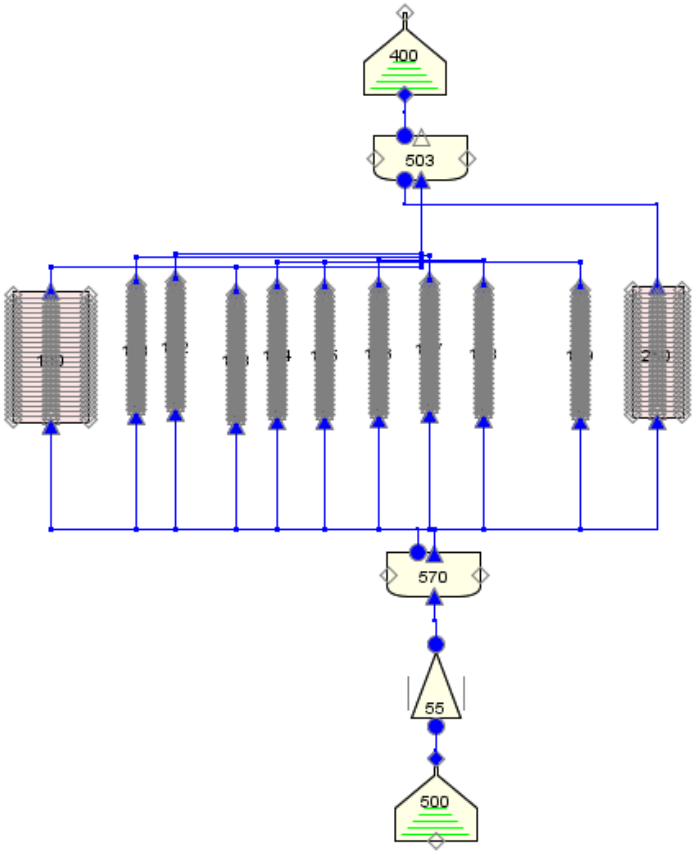

Fig. 4. SNAP representation of the RELAP5 model.

1	2	3	4	5	6	7	8	9	10	11	12	13	14	15	16	17	
						250	250	250	250	250							1
				250	250	250	100	100	100	250	250	250					2
			250	250	100	100	100	100	100	100	100	250	250				3
		250	250	100	100	100	100	100	100	100	100	100	250	250			4
	250	250	100	100	100	100	100	100	100	100	100	100	100	250	250		5
	250	100	100	100	100	100	100	100	100	100	100	100	100	100	250		6
250	250	100	100	100	100	100	100	100	100	100	100	100	100	100	250	250	7
250	100	100	100	100	100	100	100	100	100	100	100	100	100	100	100	250	8
250	100	100	100	100	100	100	100	100	100	100	100	100	100	100	100	250	9
250	100	100	100	100	100	100	100	100	100	100	100	100	100	100	100	250	10
250	250	100	100	100	100	100	100	110	111	112	113	114	100	100	250	250	11
	250	100	100	100	100	100	100	115	102	103	104	116	100	100	250		12
	250	250	100	100	100	100	100	117	105	101	106	118	100	250	250		13
		250	250	100	100	100	100	119	107	108	109	120	250	250			14
			250	250	100	100	100	121	122	123	124	250	250				15
				250	250	250	100	100	100	250	250	250					16
						250	250	250	250	250							17

Fig. 5. Thermal-hydraulic channels in model number 2.

1	2	3	4	5	6	7	8	9	10	11	12	13	14	15	16	17	
						250	250	250	250	250							1
				250	250	250	100	100	100	250	250	250					2
			250	250	100	100	100	100	100	100	100	250	250				3
		250	250	100	100	100	100	100	100	100	100	100	250	250			4
	250	250	100	100	100	100	100	100	100	100	100	100	100	250	250		5
	250	100	100	100	100	100	100	100	100	100	100	100	100	100	250		6
250	250	100	100	100	100	100	100	100	100	100	100	100	100	100	250	250	7
250	100	100	100	100	100	100	100	100	100	100	100	100	100	100	100	250	8
250	100	100	100	100	100	100	100	100	100	100	100	100	100	100	100	250	9
250	100	100	100	100	100	100	100	100	100	100	100	100	100	100	100	250	10
250	250	100	100	100	100	100	100	110	110	110	110	110	100	100	250	250	11
	250	100	100	100	100	100	100	110	102	103	104	110	100	100	250		12
	250	250	100	100	100	100	100	110	105	101	106	110	100	250	250		13
		250	250	100	100	100	100	110	107	108	109	110	250	250			14
			250	250	100	100	100	110	110	110	110	250	250				15
				250	250	250	100	100	100	250	250	250					16
						250	250	250	250	250							17

Fig. 6. Thermal-hydraulic channels in model number 3.

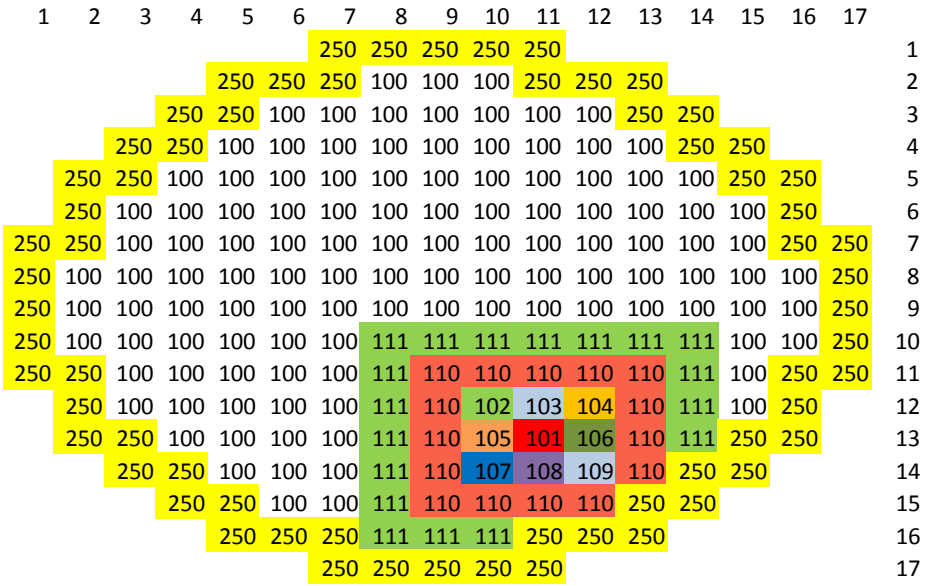

Fig. 7. Thermal-hydraulic channels in model number 4.

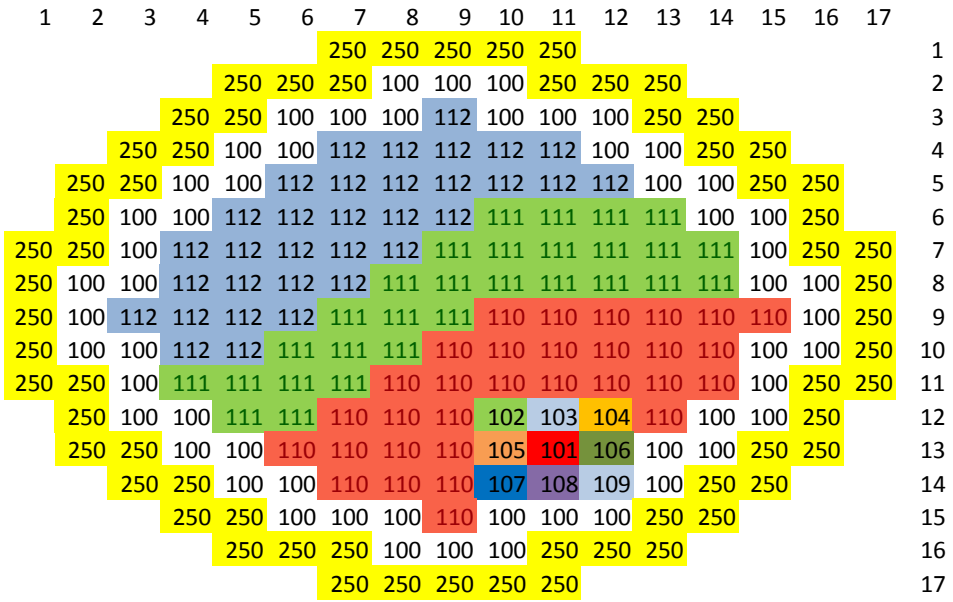

Fig. 8. Thermal-hydraulic channels in model number 5.

1	2	3	4	5	6	7	8	9	10	11	12	13	14	15	16	17	
						250	250	250	250	250							1
				250	250	250	251	252	253	250	250	250					2
			250	250	254	255	256	257	258	259	260	250	250				3
		250	250	261	262	263	264	265	266	267	268	269	250	250			4
	250	250	270	271	272	273	274	275	276	277	278	279	280	250	250		5
	250	281	282	283	284	285	286	287	288	289	290	291	292	293	250		6
250	250	294	295	296	297	298	299	300	301	302	303	304	305	306	250	250	7
250	307	308	309	310	311	312	313	314	315	316	317	318	319	320	321	250	8
250	322	323	324	325	326	327	328	329	330	331	332	333	334	335	336	250	9
250	337	338	339	340	341	342	343	344	345	346	347	348	349	350	351	250	10
250	250	352	353	354	355	356	357	358	359	360	361	362	363	364	250	250	11
	250	365	366	367	368	369	370	371	372	373	374	375	376	377	250		12
	250	250	378	379	380	381	382	383	384	385	386	387	388	250	250		13
		250	250	389	390	391	392	393	394	395	396	397	250	250			14
			250	250	398	399	400	401	402	403	404	250	250				15
				250	250	250	405	406	407	250	250	250					16
						250	250	250	250	250							17

Fig. 9. Thermal-hydraulic channels in model number 6.

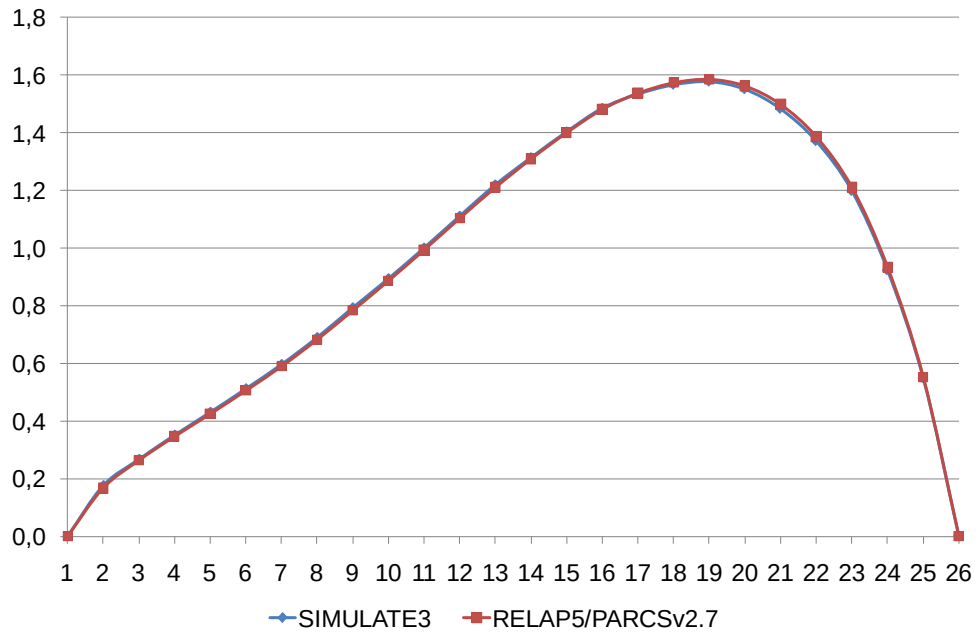

Fig. 10. Comparison of axial power profiles in initial model for the ARI case.

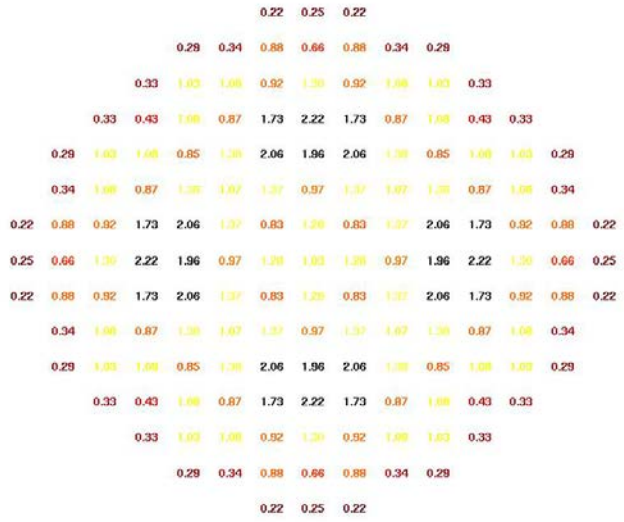

Fig. 11. Relative radial power profile in initial model for the ARI case.

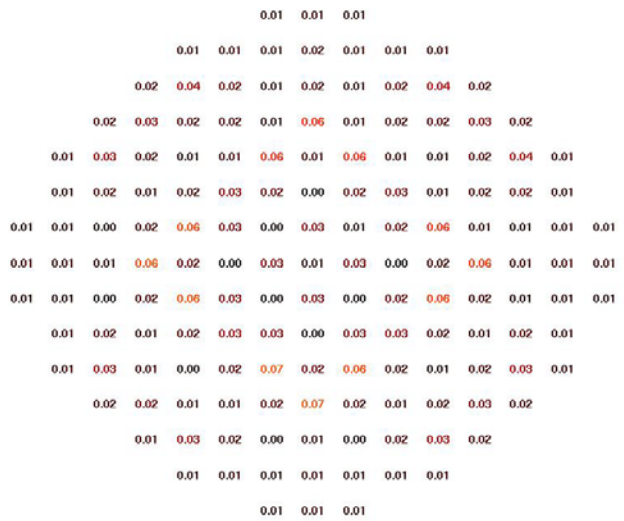

Fig. 12. Radial power profile error in initial model for the ARI case.

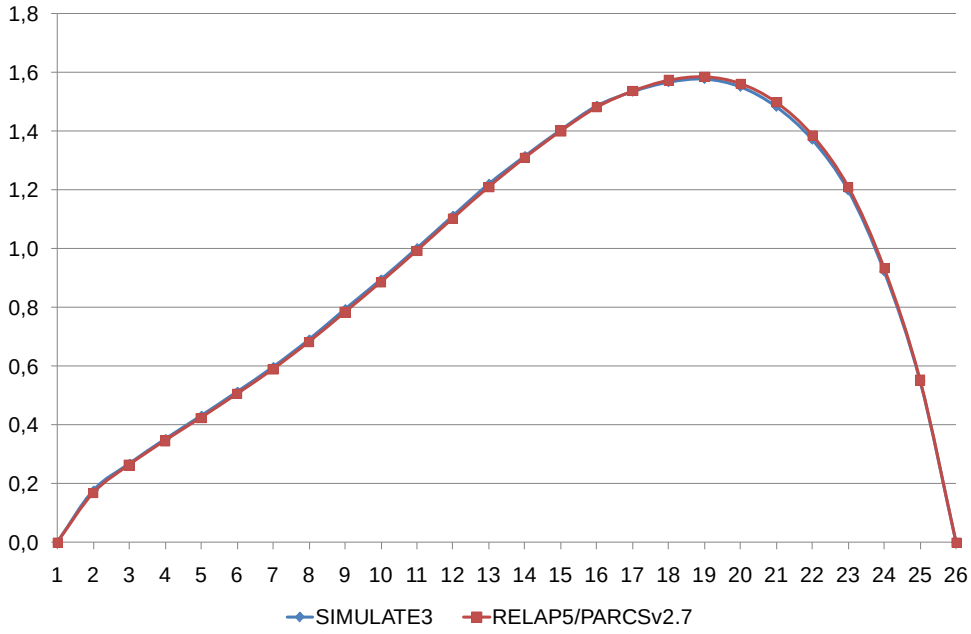

Fig. 13. Comparison of axial power profiles in model 2 for the ARI case.

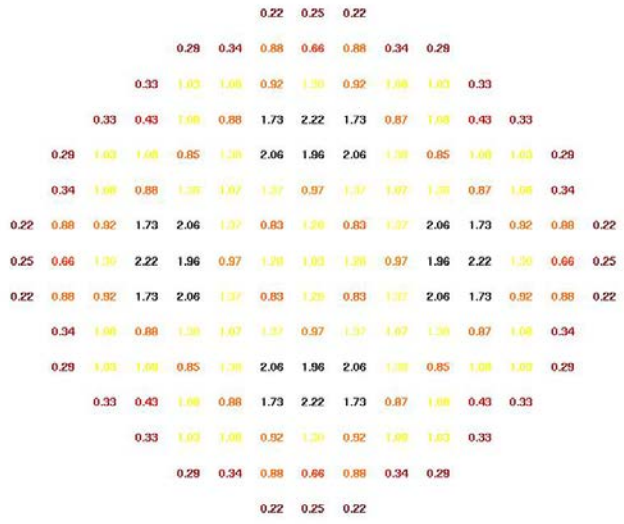

Fig. 14. Relative radial power profile in model 2 for the ARI case.

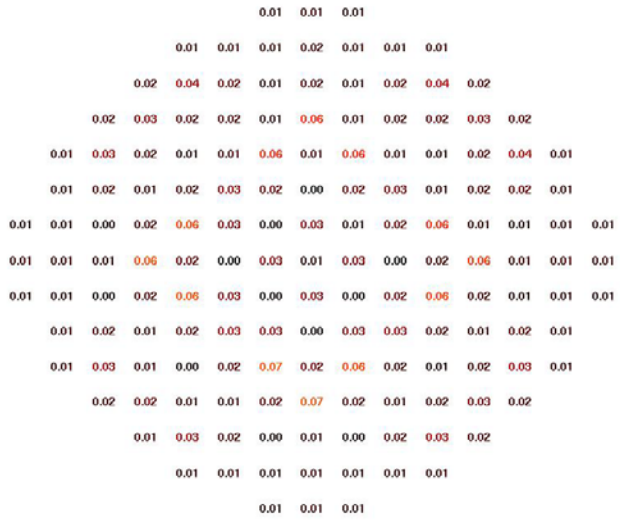

Fig. 15. Radial power profile error in model 2 for the ARI case.

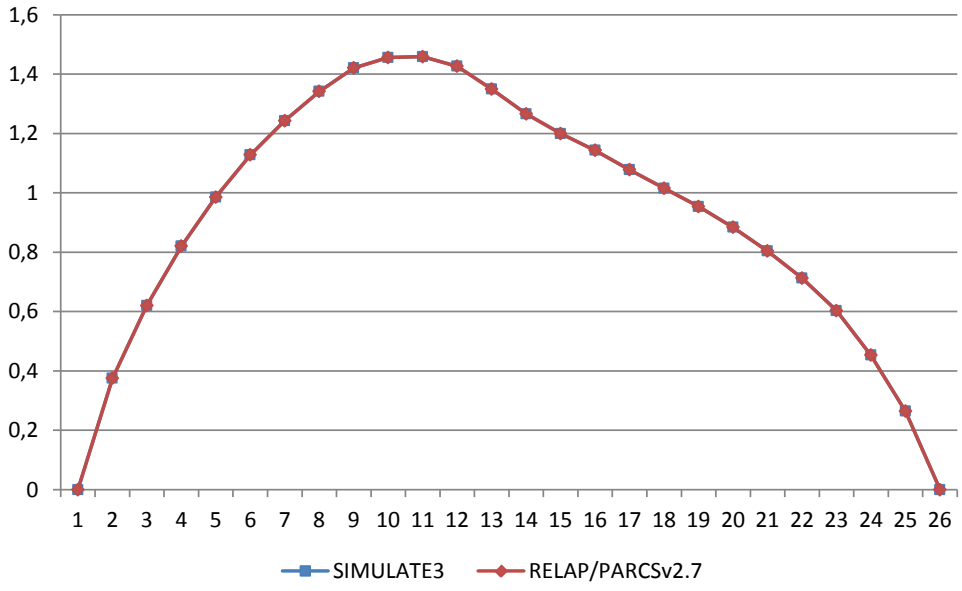

Fig. 16. Comparison of axial power profiles in initial model for the RIL case.

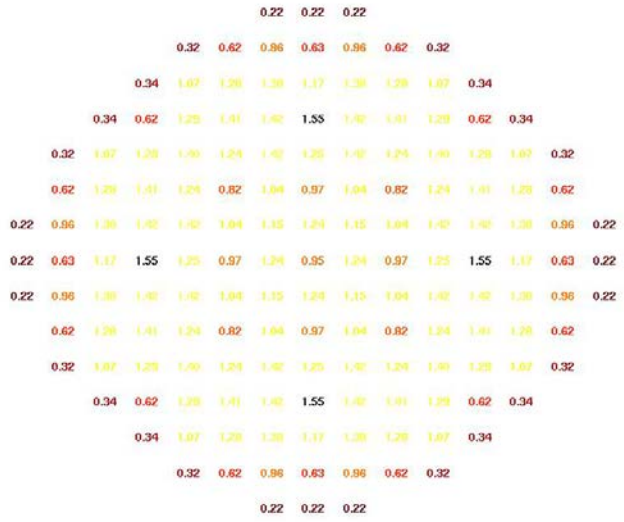

Fig. 17. Relative radial power profile in initial model for the RIL case.

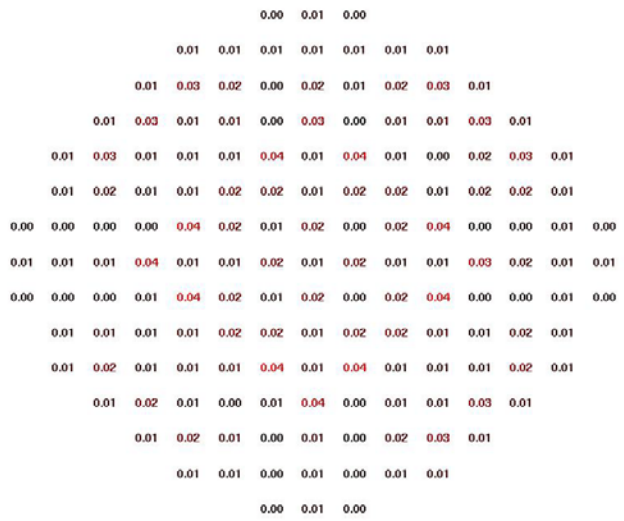

Fig. 18. Radial power profile error in initial model for the RIL case.

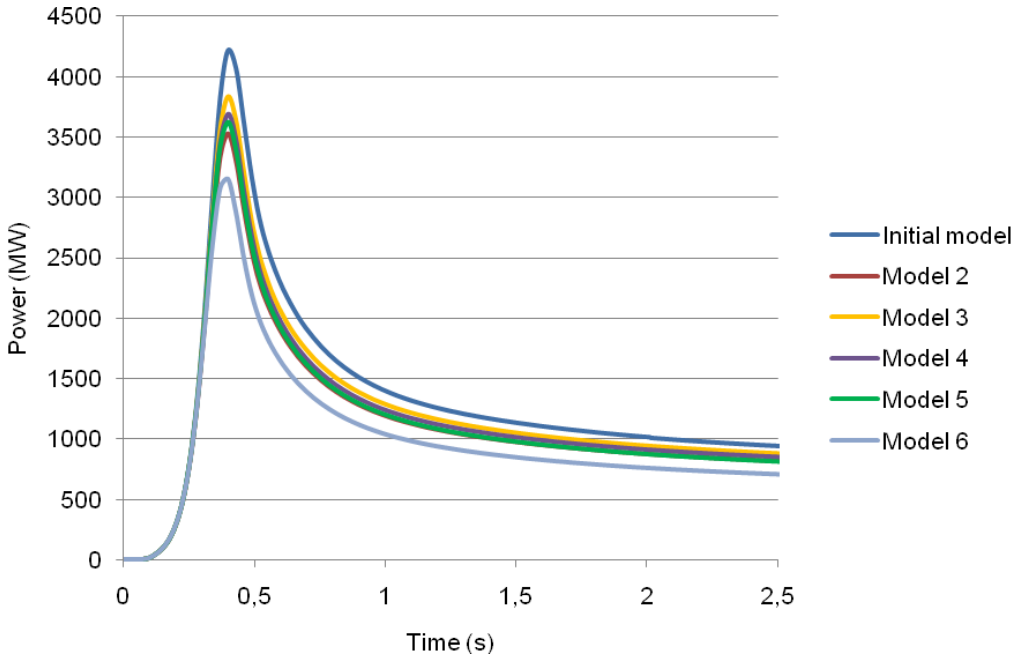

Fig.19. Total reactor power evolution comparison with ARI.

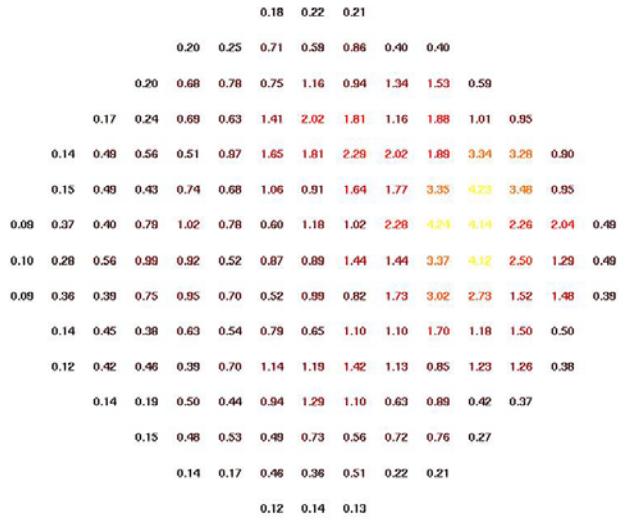

Fig 20. Relative reactor power, at maximum power, in initial model at ARI.

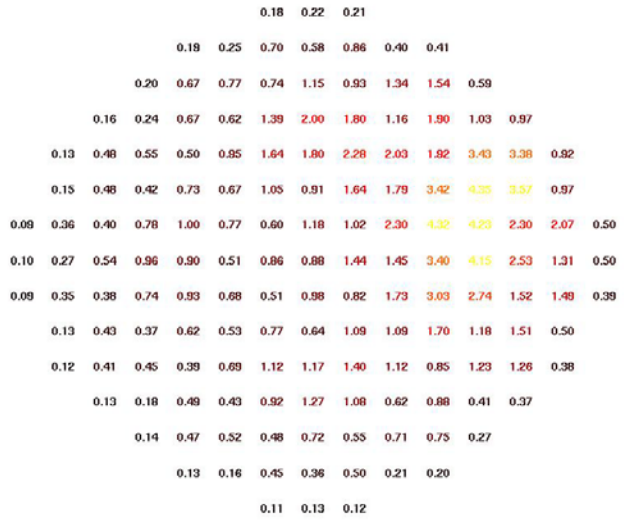

Fig 21. Relative reactor power, at maximum power, in model 6 at ARI.

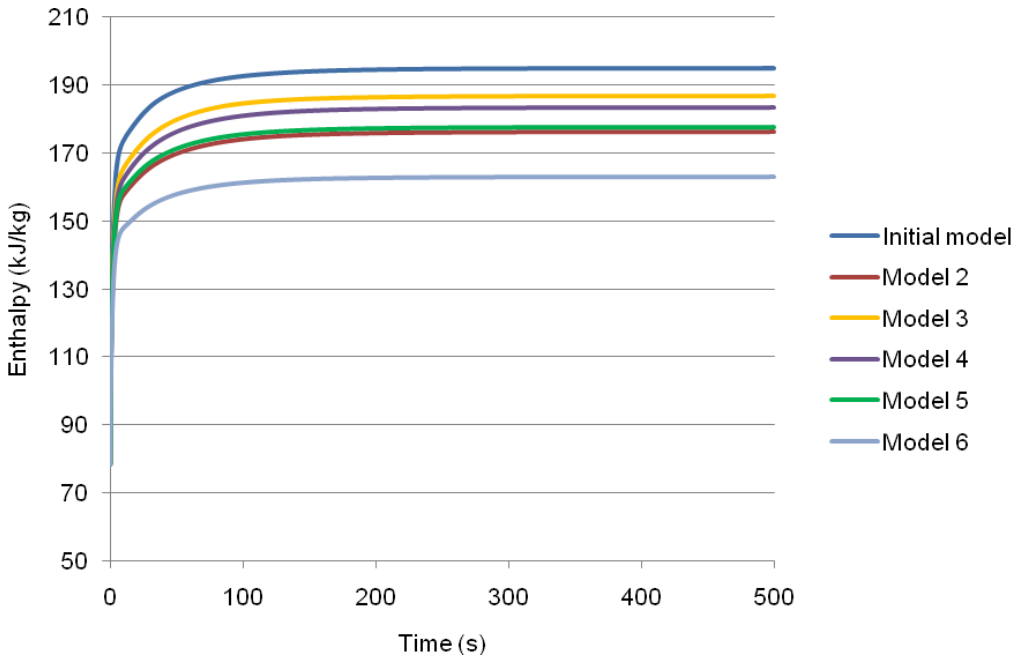

Fig. 22. Enthalpy rise evolution comparison with ARI.

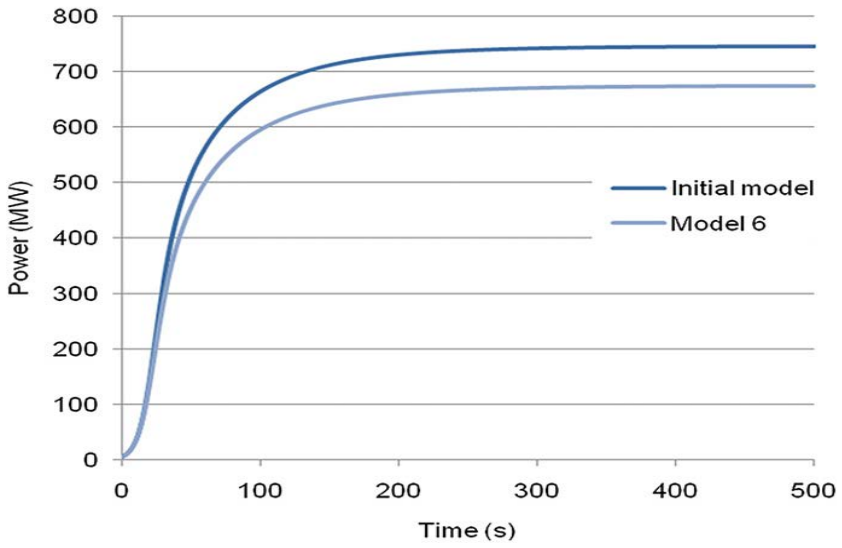

Fig. 23. Total reactor power evolution in RIL.

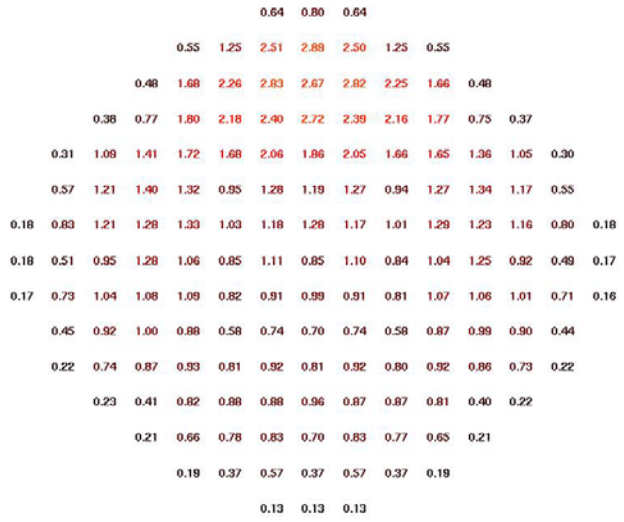

Fig 24. Relative reactor power, at 400 s, in initial model at RIL.

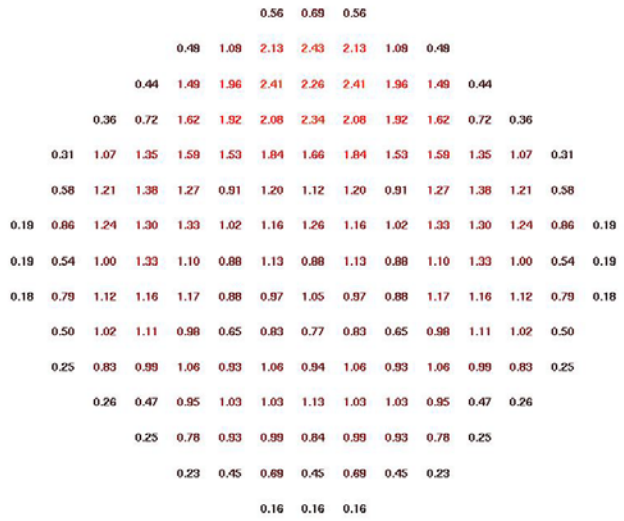

Fig 25. Relative reactor power, at 400 s, in model 6 at RIL.

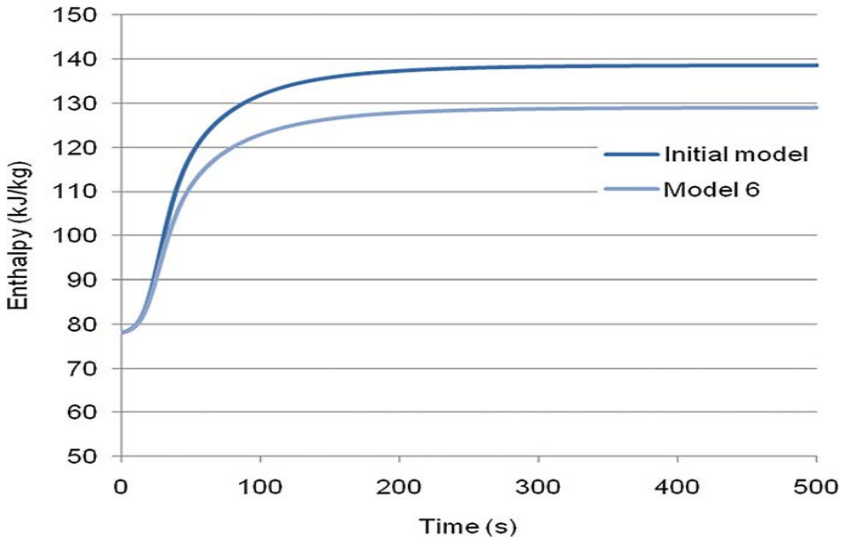

Fig 26. Enthalpy rise evolution comparison in RIL.

TABLE I

Values of β_{ef} and ejected control rod worth

Case	β_{ef}	Control rod worth (pcm/$)	Coords./bank
ARI	0.00629	720/1.145	13-11/2
RIL	0.00634	325.3/0.513	9-15/4

TABLE II

k_{eff} and *RMS* values in ARI case

Case	k_{eff} SIMULATE3	k_{eff} RELAP5/PARCS v2.7	Deviation (pcm)	*RMS* (%)
Initial	0.92997	0.930275	30.5	0.0074
Model 2	0.92997	0.930274	30.4	0.0073
Model 3	0.92997	0.930275	30.5	0.0074
Model 4	0.92997	0.930275	30.5	0.0074
Model 5	0.92997	0.930273	30.3	0.0073
Model 6	0.92997	0.930270	30.0	0.0055

TABLE III

k_{eff} and *RMS* values in RIL case

Case	k_{eff} SIMULATE3	k_{eff} RELAP5/PARCS v2.7	Deviation (pcm)	*RMS* (%)

Initial	0.98276	0.982198	56.2	0.004
Model 2	0.98276	0.982199	56.1	0.0059
Model 3	0.98276	0.982199	56.1	0.0059
Model 4	0.98276	0.982199	56.1	0.0059
Model 5	0.98276	0.982199	56.1	0.006
Model 6	0.98276	0.982198	56.2	0.004

TABLE IV

Power peak and maximum Enthalpy values with ARI

Case	Power peak (MW)	Max. Enthalpy (kJ/kg)
Initial model	4217.33	195.15
Model 2	3529.81	176.40
Model 3	3834.51	186.73
Model 4	3693.52	183.31
Model 5	3625.38	177.68
Model 6	3150.88	163.17

TABLE V

CPU Time ARI

Case	Coupled Steady-State (s)	Transient (s)
Initial model	95.2656	658.188
Model 2	180.961	1092.350
Model 3	93.975	650.602
Model 4	99.9966	664.814
Model 5	111.790	645.563
Model 6	1159.110	7630.450

TABLE VI

Maximum Power and maximum Enthalpy values with RIL

Case	Power peak (MW)	Max. Enthalpy (kJ/kg)
Initial model	744.71	138.52
Model 2	682.33	130.95
Model 3	692.23	131.92
Model 4	670.59	129.35
Model 5	664.61	130.14

Model 6	602.17	125.02

TABLE VII

CPU Time RIL

Case	Coupled Steady-State (s)	Transient (s)
Initial model	41.0	617.0
Model 2	41.0	1023.0
Model 3	43.0	634.0
Model 4	41.0	695.0
Model 5	42.0	638.0
Model 6	51.0	7360.0